Hindawi
International Journal of Mathematics and Mathematical Sciences
Volume 2023, Article ID 9134811, 14 pages
https://doi.org/10.1155/2023/9134811

Research Article

Effects of Chemical Reaction and Joule Heating on MHD Generalized Couette Flow between Two Parallel Vertical Porous Plates with Induced Magnetic Field and Newtonian Heating/Cooling

Jumanne Mng'ang'a

The Local Government Training Institute (LGTI), Dodoma, Tanzania

Correspondence should be addressed to Jumanne Mng'ang'a; jumanne.mnganga@lgti.ac.tz

Received 17 November 2022; Revised 9 January 2023; Accepted 18 January 2023; Published 9 February 2023

Academic Editor: Saranya Shekar

In this article, the effects of chemical reaction and Joule heating on MHD generalized Couette flow between two vertical porous plates with induced magnetic field and Newtonian heating/cooling have been investigated. The mathematical model used for the MHD generalized Couette flow takes into account the effect of viscous dissipation. The system of nonlinear partial differential equations governing the flow was solved numerically using the finite difference method. The resulting numerical schemes are simulated in MATLAB to obtain the profiles of the flow variables such as velocity, induced magnetic field, temperature, and concentration profiles graphically. Also, the effects of the flow parameters on the skin-friction coefficient, Nusselt number, and Sherwood number are obtained and discussed numerically through tabular forms. The findings show that an increase in the chemical reaction parameter leads to a decrease in the concentration profiles. Also, increase in the Joule heating parameter and heat generation parameter leads to an increase in the temperature profiles. Induced magnetic field profiles increase with an increase in Reynold's number. The findings of this study are important due to its application in developing a variety of chemical technologies, including polymer manufacturing, MHD pumps, food processing, chemical catalytic reactors, astronomy, MHD flow meters, and lubrication.

1. Introduction

Magnetohydrodynamic (MHD) generalized Couette flow continues to be of interest to researchers due to its various range of practical applications in lubrication, manufacturing processes, MHD power generator, polymer processing, astrophysical fluid dynamics, plasma aerodynamics, and geophysical fluid dynamics. The study of magnetohydrodynamic generalized Couette flows of different non-Newtonian fluids has been attracted by various researchers in fluid dynamics due to their applications in engineering and industry. The laminar flow of a viscous fluid between two parallel surfaces, one of which travels tangentially with respect to the other, is known as the Couette flow. This flow can be motivated by a pressure gradient that is present in the flow direction. Several scholars have investigated the magnetohydrodynamic generalized Couette flow between two parallel vertical plates. Khan et al. [1] analyzed the second law to determine how Newtonian heating affects the Couette flow of a viscoelastic dusty fluid and the transfer of heat in a rotating frame. Umavathi et al. [2] studied the Poiseuille–Couette flow with heat transfer in the inclined channel. They concluded that increases in the Grashof number, angle of inclination, and height ratio increase velocity, while increases in the Hartmann number, viscosity, and conductivity ratios decrease the velocity profiles. Bég et al. [3] analyzed the oblique magnetic field in a rotating highly permeable medium. Barikbin et al. [4] analyzed non-Newtonian fluid for MHD Couette flow using the Ritz–Galerkin method. Sreekala and Reddy [5] studied the

effect of inclined magnetic field with the steady MHD Couette flow. Joseph et al. [6] investigated heat transfer in inclined magnetic field with unsteady MHD Couette flow between two infinitely parallel porous plates. The temperature-dependent transient MHD Couette flow and heat transfer of dusty fluid were studied by Mosayebidorcheh et al. [7]. Jha et al. [8] investigated thermal radiation with unsteady MHD free convective Couette flow. Ngiangia and Okechukwu [9] discussed the impact of variable electroconductivity and radiation. They indicated that increases in electroconductivity, Prandtl number, Reynolds number, and Grashof number result in an increase in velocity distribution, while increases in the magnetic field result in a drop in velocity. Raju et al. [10] discussed the influence of diffusion thermo and thermal diffusion on a natural convection Couette flow using the finite element method. Ali et al. [11] investigated convective cooling of the nanofluids in a rotating system. Job and Gunakala [12] studied the thermal radiation for vertical permeable plates using Galerkin's finite element method. Also, Ali et al. [13] analyzed the Couette flow of a maxwell fluid for three dimensional with periodic injection/suction. Hussain et al. [14] analyzed instability of the MHD Couette flow of an electrically conducting fluid. Anyanwu et al. [15] discussed the influence of radioactive and a constant pressure gradient on an unsteady MHD Couette flow.

Chemical reaction can be categorized as homogeneous or heterogeneous reaction which can happen in a single phase or at the surface. The effects of chemical reaction depend on the order of the reaction rate for both heterogeneous and homogeneous reaction. The study of chemical reaction processes is beneficial in developing a variety of chemical technologies, including polymer manufacturing, MHD pumps, MHD flow meter, chemical catalytic reactors, and food processing. The chemical reactions have numerous applications in many sectors of science, engineering, and technology. The two-step exothermic chemical reaction of generalized Couette hydromagnetic flow with thermal criticality and entropy generation was presented by Kareem and Gbadeyan [16]. Jha and Sarki [17] analyzed the effects of Dufour and chemical reaction on a moving vertical porous plate. Soumya et al. [18] studied the effects of chemical reaction, variable thermal conductivity, and nanoparticles injection on the MHD three-dimensional free convective Couette flow. Reddy et al. [19] discussed the effects of chemical reaction and thermal radiation on an unsteady MHD Couette flow through a porous medium with periodic wall temperature. The study reveals that increasing effect of chemical reaction parameter leads to decrease in the concentration profiles. Increasing value of magnetic parameter leads to decrease in the velocity profiles. Ajibade and Umar [20] analyzed the effect of chemical reaction and radiation absorption on the unsteady MHD free convective Couette flow in a vertical channel. Apelblat [21] discussed analytically the effects of first order chemical reaction with mass transfer. Prakash et al. [22] analyzed the effects of chemical reaction and thermo-diffusion on the MHD free convective Couette flow. Abbaszadeh et al. [23] investigated the effects of two step exothermic reaction on generalized Couette hydromagnetic flow using the direct meshless local Petrov–Galerkin method. Chen and Arce [24] discussed the mathematical and numerical approach for convective-diffusive mass transfer with chemical reaction in the Couette flow. Kareem and Gbadeyan [16] studied entropy generation and thermal criticality of generalized Couette hydromagnetic flow of two-step exothermic chemical reaction in a channel. The study concluded that low-dissipation rates can promote irreversibility processes and low-heat source terms can reduce thermal explosion.

An electric current flows through a resistance, it can be said to "Joule heating" the object being passed through. Joule heating is important due to its various applications including portable fan heater, bulb that emits light, clothes iron, and the hot flow produced by a hairdryer. Sarkar [25] investigated the MHD Couette–Poiseuille flow with laminar forced convection and viscous and Joule dissipations. Zueco et al. [26] studied the effects of Joule heating, Hall and ion slip in a non-Darcian porous media channel with a nonlinear transient hydromagnetic partially ionized the dissipative Couette flow. Ramesh [27] analyzed the effects of Joule heating and viscous dissipation on a Jeffrey fluid's Couette and Poiseuille flows by taking into account the slip boundary conditions. Bég et al. [28] analyzed numerically the effects of Hall current, Joule heating, viscous flow, and Ion slip on magnetohydrodynamic Hartmann–Couette flow and heat transfer in a Darcian channel. Saleel et al. [29] discussed the microfluidics flow control using the electro-osmotic Couette flow and Joule heating. Shamshuddin et al. [30] investigated the effects of Joule heating and viscous dissipation in non-Fourier MHD squeezing flow, as well as heat and mass transfer between Riga plates with thermal radiation. Shamshuddin and Satya Narayana [31] studied the effect of viscous dissipation and Joule heating combined with a Cattaneo–Christov heat flux on MHD flow past a Riga plate.

Induced magnetic on the hydromagnetic generalized Couette flow is beneficial in MHD pumps and MHD flow meters. The effects of induced magnetic field have numerous applications in many sectors of science, engineering, and technology. The magnetic field is modified by the induced magnetic field, which also creates its own magnetic field in the fluid. The flow of the fluid through the magnetic field also generates mechanical forces that change the fluid's motion. Consequently, it is necessary to include the influence of the induced magnetic field in the hydromagnetic equations in a number of physical conditions. In the metallurgical sector, magnetic fields are employed for stirring, heating liquid metals, and levitating. Sarveshanand and Singh [32] discussed the effects of induced magnetic field on magnetohydrodynamic free convection between vertical parallel porous plates. The study concluded that increasing suction parameter leads to decrease the induced current density and velocity field and while it has increasing effect on the induced magnetic field. Mng'ang'a et al. [33] investigated the effects of induced magnetic field in the direction of the fluid flow on hydromagnetic surface driven flow. Kwanza and Balakiyema [34] analyzed the magnetic induction on MHD free convective flow past an infinite vertical porous plate. The study reveals that the increase of the Prandtl number and the

suction velocity lead to a decrease in the temperature, induced magnetic field and velocity profiles in the boundary layer region whereas increase in the magnetic field parameter and Grashof number leads to increased induced magnetic field profiles. Singh et al. [35] discuss the effects of induced magnetic field on hydromagnetic free convection. Akbar et al. [36] investigated the effects of induced magnetic field on interaction of nanoparticles for the peristaltic flow in an asymmetric channel. Sher Akbar et al. [37] discuss the effects of induced magnetic field and heat flux in a permeable channel.

The novelty of this work is to investigate the combined effects of chemical reaction and Joule heating on the MHD generalized Couette flow between two parallel vertical porous plates with induced magnetic field and Newtonian heating/cooling by taking into the account the effects of viscous dissipation. The system of nonlinear partial differential equation of the governing equations was obtained using the finite difference method and implemented in MATLAB. The effects of various dimensionless parameters on velocity profiles, temperature profiles, concentration profiles, and induced magnetic field profiles are discussed in detail. The results of this problem can be helpful in various science and engineering. The results of this problem can be helpful in various devices subject to significant variations in the gravitational force, its application on heat exchanger designs, wire and glass fiber drawings, and its application in nuclear engineering in connection with reactor cooling. In line with the aforementioned objectives and aim, this study proposes answers to the following research questions.

(i) How does the flow variables such as temperature, velocity, concentration, and induced magnetic field profiles varies with Prandtl number, Schmidt number, Grashof numbers for heat and mass transfer, Eckert number, Joule heating parameter, heat generation parameter, Reynold's number, magnetic Prandtl number, suction/injection parameter, permeability parameter, chemical reaction parameter, and magnetic parameter?

(ii) What are the variations in the Sherwood number, Nusselt number, and skin friction coefficient due to the enrichment in Joule heating parameter, heat generation parameter, Reynold's number, Prandtl number, Schmidt number, Grashof numbers for heat and mass transfer, Eckert number, magnetic Prandtl number, suction/injection parameter, magnetic parameter, chemical reaction parameter, and permeability parameter?

2. Mathematical Formulation

Let us consider the bidimensional unsteady laminar flow of incompressible, electrically conducting, and viscous between two infinite parallel vertical porous plates with magnetic field strength vector ($\overrightarrow{B} = (B_x, B_y)$), constant suction velocity $u = u_o$, and a constant magnetic field B_0 applied perpendicular to the plates as depicted in Figure 1. Fluid flow

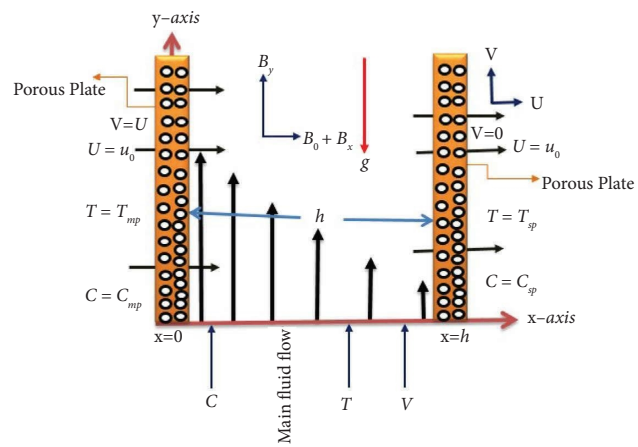

Figure 1: Schematic diagram of the physical system.

between two parallel vertical porous plates with infinite lengths at $x = 0$ and $x = h$.

The fluid is flowing through a porous medium that is assumed to obey Darcy's law. Electrically conducting fluid produce induced currents then produce an induced magnetic field ($\overrightarrow{B_x}$ and $\overrightarrow{B_y}$) in x and y direction, respectively, that opposite the applied field, resisting the conductor's motion.

At initial concentration $C = C_{sp}$ and temperature $T = T_{sp}$ at time $t \leq 0$, the fluid is initially stationary, as are the plates at $x = 0$ and $x = h$. When $t > 0$, the porous plate at $x = 0$ begins to move impulsively in its own plane at a constant velocity of U, and its concentration and temperature rise to $T = T_{mp}$ and $C = C_{mp}$, respectively. In contrast, the other porous plate, which is located at a distance of h from it, remains fixed and maintains its concentration and temperature at $C = C_{sp}$ and $T = T_{sp}$. The concentration, induced magnetic profile, temperature, and velocity are functions of x and t since the porous plates have an unlimited length. In the $x-$ direction, the fluid is suctioned with constant velocity u_0.

The unsteady MHD Couette flow between two vertical porous plates is governed by the following nonlinear partial differential equations. Using Boussinesq's approximation, the governing equations for the current physical system in dimensional form are as follow [8]:-

Continuity equation

$$\frac{\partial u}{\partial x} = 0. \tag{1}$$

Momentum equation

$$\frac{\partial V}{\partial t} + u_0 \frac{\partial V}{\partial x} = -\frac{\mu}{\rho k_p} V + \nu \frac{\partial^2 V}{\partial x^2} + \beta_*^t g\left(T - T_{sp}\right) + \beta_*^c g\left(C - C_{sp}\right) - \frac{\sigma\left(u_o B_y B_0 + u_o B_y B_x - V B_0^2 - 2V B_0 B_x - V B_x^2\right)}{\rho}. \tag{2}$$

Energy Equation

$$\frac{\partial T}{\partial t}+u_0\frac{\partial T}{\partial x}=\frac{k}{\rho C_p}\left(\frac{\partial^2 T}{\partial x^2}\right)+\frac{H\left(T-T_{sp}\right)}{\rho C_p}+\frac{\mu}{\rho C_p}\left(\frac{\partial V}{\partial x}\right)^2+\frac{\sigma}{\rho C_p}\left(u_o B_y-V\left(B_0+B_x\right)\right)^2. \tag{3}$$

Concentration equation

$$\frac{\partial C}{\partial t}+u_0\frac{\partial C}{\partial x}=D_m\frac{\partial^2 C}{\partial x^2}-k_r\left(C-C_{sp}\right)^2. \tag{4}$$

Equation of magnetic induction

$$\frac{\partial B_x}{\partial t}=\frac{\partial B_y}{\partial y}u_0-\frac{\partial V}{\partial y}B_0-\frac{\partial V}{\partial y}B_x-\frac{\partial B_x}{\partial y}V+\frac{1}{\mu_e\sigma}\left(\frac{\partial^2 B_x}{\partial x^2}+\frac{\partial^2 B_x}{\partial y^2}\right), \tag{5}$$

$$\frac{\partial B_y}{\partial t}=-\frac{\partial B_y}{\partial x}u_0+\frac{\partial V}{\partial x}B_0+\frac{\partial V}{\partial x}B_x+\frac{\partial B_x}{\partial x}V+\frac{1}{\mu_e\sigma}\left(\frac{\partial^2 B_y}{\partial x^2}+\frac{\partial^2 B_y}{\partial y^2}\right). \tag{6}$$

The corresponding initial and boundary conditions are as follows[8]:-

$$\begin{aligned}
&t>0:\ \begin{cases} V=U, & T=T_{mp}, \quad C=C_{mp}, \quad B_x=B_y=B_0 \text{ at } x=0,\\ V=0, & T=T_{sp}, \quad C=C_{sp}, \quad B_x=B_y=0 \text{ at } x=h,\end{cases}\\
&t\le 0:\ V=0, T=T_{sp}, C=C_{sp}, B_x=B_y=0 \text{ for } 0\le x\le h.
\end{aligned} \tag{7}$$

To nondimensionalize the governing equations, we use the following dimensionless quantities for the present hydromagnetic problem

$$\begin{aligned}
&B_x=B_x^*B_0, \quad V=UV^*, \quad t=\frac{h^2t^*}{\nu}, x=hx^*, y=hy^*,\\
&B_y=B_y^*B_0, T=T_{sp}+\theta\left(T_{mp}-T_{sp}\right), \quad C=C_{sp}+\phi\left(C_{mp}-C_{sp}\right).
\end{aligned} \tag{8}$$

Using the dimensionless variables defined in equations (2)–(6) and (8) in nondimensional forms are as follows:-

$$\frac{\partial V^*}{\partial t^*}+\mathrm{Re}.S\frac{\partial V^*}{\partial x^*}=-XV^*+\frac{\partial^2 V^*}{\partial x^{*^2}}+Gr\theta+Gc\phi-M\left(SB_y^*+SB_y^*B_x^*-V^*-2V^*B_x^*-V^*B_x^{*^2}\right), \tag{9}$$

$$\begin{aligned}
\frac{\partial\theta}{\partial t^*}+ReS\frac{\partial\theta}{\partial x^*}=&\frac{1}{\mathrm{Pr}}\left[\frac{\partial^2\theta}{\partial x^{*^2}}\right]+Q\theta+Ec\left(\frac{\partial V^*}{\partial x^*}\right)^2+J\left(SB_y^{*^2}-2V^*B_y^*-2V^*B_y^*B_x^*\right)\\
&+\frac{J}{S}\left(V^{*^2}+2V^{*^2}B_x^*+V^{*^2}B_x^{*^2}\right),
\end{aligned} \tag{10}$$

$$\frac{\partial\phi}{\partial t^*}+\mathrm{Re}S\frac{\partial\phi}{\partial x^*}=\frac{1}{Sc}\frac{\partial^2\phi}{\partial x^{*^2}}-K\phi^2, \tag{11}$$

$$\frac{\partial B_x^*}{\partial t^*} = \mathrm{Re}.S\frac{\partial B_y^*}{\partial y^*} - \mathrm{Re}\frac{\partial B_y^*}{\partial y^*}V^* + \frac{1}{\mathrm{Prm}}\left(\frac{\partial^2 B_x^*}{\partial x^{*^2}} + \frac{\partial^2 B_x^*}{\partial y^{*^2}}\right), \tag{12}$$

$$\frac{\partial B_y^*}{\partial t^*} = -\mathrm{Re}.S\frac{\partial B_y^*}{\partial x^*} + \mathrm{Re}B_x^*\frac{\partial V^*}{\partial x^*} + \mathrm{Re}\frac{\partial V^*}{\partial x^*} + \frac{\partial B_x^*}{\partial x^*} + \mathrm{Re}\frac{\partial B_x^*}{\partial x^*}V^* + \frac{1}{\mathrm{Prm}}\left(\frac{\partial^2 B_y^*}{\partial x^{*^2}} + \frac{\partial^2 B_y^*}{\partial y^{*^2}}\right), \tag{13}$$

where $J = B_0^2\sigma h^2 u_0/\nu\rho c_p$ represents Joule heating parameter, $M = B_0^2\sigma h^2/\nu\rho$ represents magnetic parameter, $S = u_0/U$ represents injection/suction parameter, $X = h^2/k_p$ represents the permeability parameter, $\mathrm{Re} = Uh/\nu$ represents the Reynolds number, $Ec = U^2/c_p(T_{mp} - T_{sp})$ represents Eckert number, $K = k_r h^2(C_{mp} - C_{sp})/\nu$ represents chemical reaction parameter, $Sc = \nu/D$ represents Schmidt number, $\mathrm{Pr} = \mu c_p\nu/k$ represents Prandtl number, $Q = h^2 H/\rho\nu c_p$ represents internal heat generation parameter, $\mathrm{Prm} = \mu_e\sigma\nu$ represents magnetic Prandtl number, $Gr = g\beta_*^t h^2(T_{mp} - T_{sp})/\nu U$ represents Grashof number for heat transfer, and $Gc = g\beta_*^c h^2(C_{mp} - C_{sp})/\nu U$ represents Grashof number for mass transfer.

The corresponding initial and boundary conditions are as follows:

$$\begin{aligned} &t^* > 0: \begin{cases} V^* = 1, \quad \theta = 1, \quad \phi = 1, \quad B_x^* = B_y^* = 1 \text{at } x^* = 0, \\ V^* = 0, \quad \theta = 0, \quad \phi = 0, \quad B_x^* = B_y^* = 0 \text{ at } x^* = 1, \end{cases} \\ &t^* \le 0: V^* = 0, \theta = 0, \phi = 0, B_x^* = B_y^* = 0 \text{ for } 0 \le x^* \le 1. \end{aligned} \tag{14}$$

3. Numerical Solution

The governing (9)–(13) are nonlinear partial differential equations, therefore cannot be solved analytically. The numerical method for nonlinear partial differential equations of momentum, concentration, energy, and induced given in (9)–(13) are solved using the finite difference method subject to the initial and boundary condition (14). The condition for time stability is the Courant–Friedrichs–Lewy or CFL condition which depends on space and time discretization. A mesh is fixed at $\Delta x = 0.3$ and $\Delta t = 0.0001$ to ensure the stability and convergence. The transport equations (9)–(13) at the grid point (i, j) are expressed in difference form using Taylor's series expansion. Thus, the values of V, C, Hx, Hy, and T at grid point $t = 0$ are known; hence the velocity, induced magnetic field, concentration, and temperature fields have been solved at time $t_{i+1} = t_i + \Delta t$ using the known values of the previous time $t = t_i$ for all $i = 1, 2, \ldots M - 1$. These processes are repeated till the required solution of velocity, induced magnetic field, concentration, and temperature field is converge.

The forward time central in space is used as the numerical scheme, in finite difference form can be approximated as

$$\begin{aligned} &T = T_j^k, C = C_j^k, V = V_j^k, \\ &\frac{\partial T}{\partial t} = \frac{T_j^{k+1} - T_j^k}{\Delta t}, \frac{\partial C}{\partial t} = \frac{C_j^{k+1} - C_j^k}{\Delta t}, \frac{\partial V}{\partial t} = \frac{V_j^{k+1} - V_j^k}{\Delta t}, \\ &\frac{\partial T}{\partial x} = \frac{T_{j+1}^k - T_{j-1}^k}{2\Delta x}, \frac{\partial C}{\partial x} = \frac{C_{j+1}^k - C_{j-1}^k}{2\Delta x}, \frac{\partial V}{\partial x} = \frac{V_{j+1}^k - V_{j-1}^k}{2\Delta x}, \\ &\frac{\partial^2 T}{\partial x^2} = \frac{T_{j+1}^k - 2T_j^k + T_{j-1}^k}{(\Delta x)^2}, \frac{\partial^2 C}{\partial x^2} = \frac{C_{j+1}^k - 2C_j^k + C_{j-1}^k}{(\Delta x)^2}, \frac{\partial^2 V}{\partial x^2} = \frac{V_{j+1}^k - 2V_j^k + V_{j-1}^k}{(\Delta x)^2}. \end{aligned} \tag{15}$$

Using equation (15) into equations (9)–(12), in finite difference form the governing equations becomes

$$
\begin{aligned}
V_j^{k+1} &= V_j^k - \Delta t \mathrm{Re}.S\left[\frac{V_{j+1}^k - V_{j-1}^k}{2\Delta x}\right] - XV_j^k\Delta t + \Delta t\left(\frac{V_{j+1}^k - 2V_j^k + V_{j-1}^k}{(\Delta x)^2}\right) \\
&\quad + GrT_j^k\Delta t + GcC_j^k\Delta t - M\left(S.By_j^k + S.By_j^k Bx_j^k - V_j^k - 2V_j^k Bx_{y_j}^k - V_j^k\left(Bx_j^k\right)^2\right)\Delta t, \\
T_j^{k+1} &= T_j^k - ReS\Delta t\left(\frac{T_{j+1}^k - T_{j-1}^k}{2\Delta x}\right) + \frac{\Delta t}{\mathrm{Pr}}\left(\frac{T_{j+1}^k - 2T_j^k + T_{j-1}^k}{(\Delta x)^2}\right) + Ec\Delta t\left[\frac{V_{j+1}^k - V_{j-1}^k}{2\Delta x}\right]^2 \\
&\quad + QT_j^k + J\left(S\left(By_j^k\right)^2 - 2V_j^k By_j^k - 2V_j^k Bx_j^k By_j^k\right) + \frac{J}{S}\left(\left(V_j^k\right)^2 + 2\left(V_j^k\right)^2 Bx_j^k + \left(V_j^k\right)^2\left(By_j^k\right)^2\right), \\
C_j^{k+1} &= C_j^k - ReS\Delta t\left[\frac{C_{j+1}^k - C_{j-1}^k}{2\Delta x}\right] + \frac{\Delta t}{Sc}\left[\frac{C_{j+1}^k - 2C_j^k + C_{j-1}^k}{(\Delta x)^2}\right] - K\Delta t\left(C_j^k\right)^2, \\
Bx_j^{k+1} &= Bx_j^k - ReS\Delta t\left[\frac{By_{j+1}^k - By_{j-1}^k}{2\Delta y}\right] - \mathrm{Re}\Delta t\left[\frac{By_{j+1}^k - By_{j-1}^k}{2\Delta y}\right]V_j^k + \frac{\Delta t}{\mathrm{Pr}_m}\left[\frac{Bx_{j+1}^k - 2Bx_j^k + Bx_{j-1}^k}{(\Delta x)^2}\right] \\
&\quad + \frac{\Delta t}{\mathrm{Pr}_m}\left[\frac{Bx_{j+1}^k - 2Bx_j^k + Bx_{j-1}^k}{(\Delta y)^2}\right], \\
By_j^{k+1} &= By_j^k + \mathrm{Re}S\Delta t\left[\frac{By_{j+1}^k - By_{j-1}^k}{2\Delta x}\right] + \mathrm{Re}Bx_j^k\Delta t\left[\frac{V_{j+1}^k - V_{j-1}^k}{2\Delta x}\right] + \mathrm{Re}\Delta t\left[\frac{V_{j+1}^k - V_{j-1}^k}{2\Delta x}\right] \\
&\quad + \mathrm{Re}\Delta t\left(\frac{Bx_{j+1}^k - Bx_{j-1}^k}{2\Delta x}\right)V_j^k + \frac{\Delta t}{\mathrm{Pr}_m}\left[\frac{By_{j+1}^k - 2By_j^k + By_{j-1}^k}{(\Delta x)^2}\right] + \frac{\Delta t}{\mathrm{Pr}_m}\left[\frac{By_{j+1}^k - 2By_j^k + By_{j-1}^k}{(2\Delta y)^2}\right].
\end{aligned}
\tag{16}
$$

Subject to the following initial and boundary conditions

$$
\begin{aligned}
&t > 0: \begin{cases} V(0,k) = 1, \quad T(0,k) = 1, \quad C(0,k) = 1, \quad Bx(0,k) = By(0,k) = 1 \text{ at } j = 0, \\ V(j,0) = 0, \quad T(j,0) = 0, \quad C(j,0) = 0, \quad Bx(j,0) = By(j,0) = 0 \text{ for all } j = 0, \end{cases} \\
&t \le 0: V(j,0) = 0, T(j,0) = 0, C(j,0) = 0, Bx(j,0) = By(j,0) = 0 \text{ for all } j = 0.
\end{aligned}
\tag{17}
$$

For practical engineering application and design, the quantities of interest are Sherwood number (Sh), skin friction coefficient (C_f), and Nusselt number (Nu) which are defined as

$$
\begin{aligned}
Sh &= \frac{x' q_m}{C_{mp} - C_{sp}}, \\
Nu &= \frac{x' q_h}{T_{mp} - T_{sp}}, \\
C_f &= \frac{x' \tau_w}{\rho U \nu},
\end{aligned}
\tag{18}
$$

where $q_m = -(\partial C/\partial x)_{x=0,1}$, $q_h = -(\partial T/\partial x)_{x=0,1}$, and $\tau_w = \mu(\partial V/\partial x)_{x=0,1}$

Substituting equation (8) into equation (18), we obtain

$$
Sh\mathrm{Re}_x^{-1} = -\left(\frac{\partial \phi}{\partial x^*}\right)_{x^*=0,1}, Nu\mathrm{Re}_x^{-1} = -\left(\frac{\partial \theta}{\partial x^*}\right)_{x^*=0,1}, C_f = \left(\frac{\partial V^*}{\partial x^*}\right)_{x^*=0,1}. \tag{19}
$$

Both temperature, velocity, concentration, and induced magnetic field profiles were obtained and utilized to compute numerical values of the Sherwood number, skin friction coefficient, and Nusselt number in equation (19).

4. Results and Discussion

To investigate the physical significance of the modeled MHD generalized Couette flow, the influence of various physical parameters involved in the problem such as Joule heating parameter, heat generation parameter, Reynold's number, Prandtl number, Schmidt number, Grashof numbers for heat and mass transfer, Eckert number, magnetic Prandtl number, suction/injection parameter, magnetic parameter, chemical reaction parameter, and permeability parameter on the nondimensional temperature, velocity, concentration, and induced magnetic field profiles are evaluated numerically and executed graphically and discussed to get the physical insight into the problem, whilst the numerical values for skin friction coefficient, Nusselt, and Sherwood numbers are represented in the tabular form. The numerical solutions have been conducted by adopting the default values of various involved physical parameters in the problem such as $\mathrm{Re} = 0.2, \mathrm{Pr} = 0.71, Sc = 0.22, Gr = 1, Gc = 1, Ec = 0.22, \mathrm{Prm} = 0.5, S = 3, M = 3, K = 0.05, J = 1, Q = 2$, and $X = 2$ until otherwise specified particularly.

Figure 2 depicts the effects of Grashof number for mass transfer (Gc) on velocity profiles. Graphically, it is observed that the velocity of the fluid increases with an increase in the Grashof number for mass transfer (Gc), since Grashof number for mass transfer represents the ratio of the species buoyancy force to the viscous force. Physically, increasing Grashof number leads to a decrease in the viscosity of the fluid which results to a decrease in the viscous force which leads to an increase in the species Bouyant force and thus increase the velocity of the fluid.

Figure 3 depicts the effects of Grashof number for heat transfer (Gr) on velocity profiles. Graphically, it is observed that increasing the values of Grashof number for heat transfer (Gr) leads to an increase in the velocity profiles. By definition, Grashof number for heat transfer represents the ratio of the thermal buoyancy force to the viscous force. Physically, increasing the Grashof number reduces the viscous force and increase thermal buoyancy force thus leads to an increase in the velocity profiles.

The effect of magnetic parameter (M) on velocity profiles is shown in Figure 4. Graphically, it is observed that increasing the values of the magnetic parameter leads to a decrease in the velocity profiles, since magnetic parameter represents the ratio of electromagnetic force to an inertia force. Physically, increasing magnetic parameter leads to an increase in the electromagnetic force which caused by the magnetic field that control the fluid flow characteristics. The presence of a magnetic field in an electrically conducting fluid enhance the Lorentz force which acts against to the fluid flow when the magnetic field is applied normal to the direction of the fluid flow which leads to a slowly the motion fluid and thus decrease the velocity of the fluid.

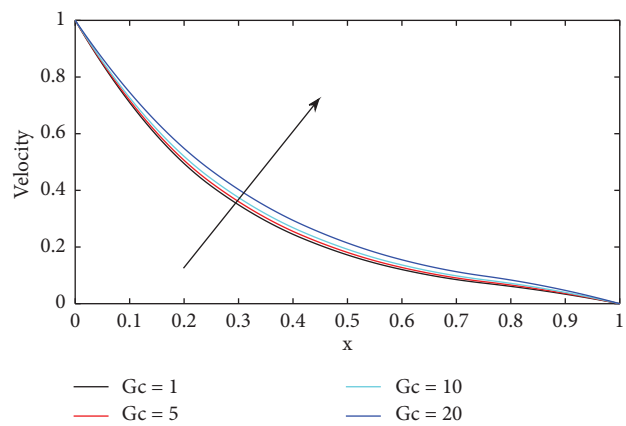

Figure 2: Velocity profiles for different values of Gc.

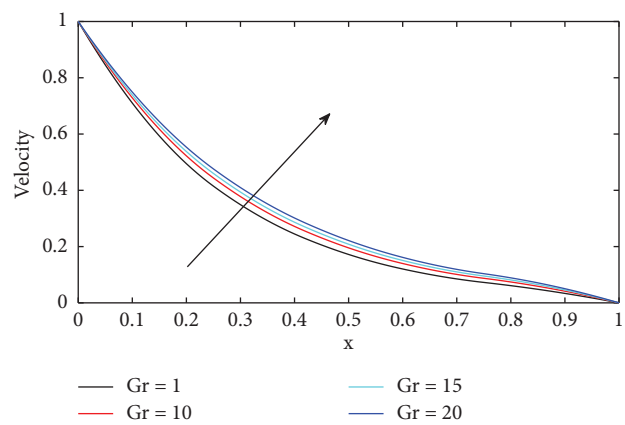

Figure 3: Velocity profiles for different values of Gr.

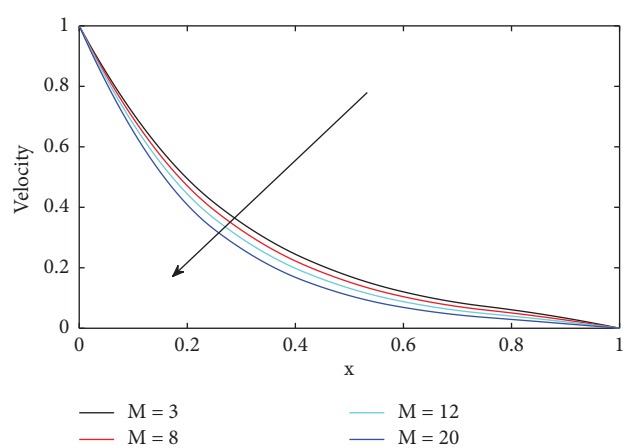

Figure 4: Velocity profiles for different values of M.

Figure 5 illustrates the effects of permeability parameter (X) on velocity profiles. Graphically, it is observed that increasing the values of the permeability parameter (X) leads to a decrease in the velocity profiles. Physically, increasing the permeability parameter which opposes the flow and leads to enhance deceleration of the flow. Therefore,

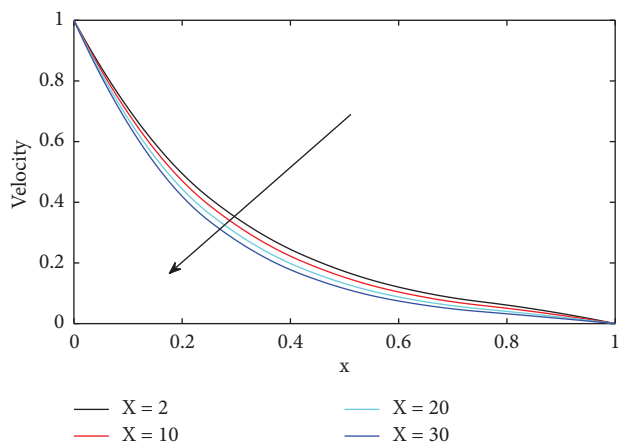

Figure 5: Velocity profiles for different values of X.

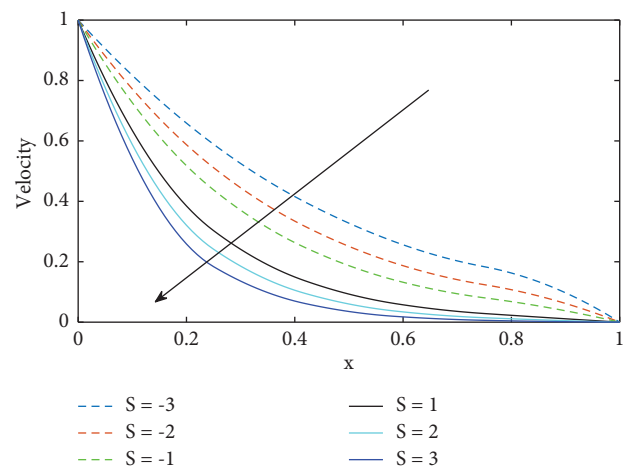

Figure 6: Velocity profiles for different values of S.

with an increase in the permeability parameter causes the resistance to the fluid motion which resulted to decrease the velocity boundary layer and thus the velocity profiles decrease.

The effects of suction/injection parameter (S) on velocity profiles are shown in Figure 6. Graphically, it is observed that increasing the values of the suction parameter ($S < 0$) leads to a decrease in the velocity of the fluid. The injection parameter ($S > 0$) increases with a decrease in the velocity of the fluid. Physically, increasing suction parameter (S) implies the removal of the fluid from the flow system which causes destabilization the velocity boundary layer leads to a decrease in the motion of the fluid and thus decrease the velocity profiles.

Figure 7 exhibits the effects of the Reynolds number (Re) on velocity profiles. Graphically, it is observed that increasing the values of the Reynolds number (Re) leads to an increase in the velocity profiles, since the Reynolds number represents the ratio of inertia force to the viscous force. Physically, increasing the Reynolds number reduces the viscous forces in the fluid and thus result to an increase in the velocity profiles.

Figure 8 presents the effects of chemical reaction parameter (K) on concentration profiles. Graphically, it is observed that increasing the values of the chemical reaction parameter (K) leads to a decrease in the fluid concentration. The positive values of K indicate the destructive type of the chemical reaction. The influence of a destructive chemical reaction parameter ($K > 0$) caused a decrease in the concentration diffusion species. Physically, increasing chemical reaction for destructive results to molecular motion become higher, which enhances the transport phenomenon, thus decreases the concentration profiles.

Figure 9 illustrates the effects of suction/injection (S) on concentration profiles. Graphically, it is observed that increasing the values of the suction (S) leads to a decrease in the concentration profiles. Physically, increasing suction/injection parameter (S) results in the thinning of the concentration boundary layer of the fluid flow which leads to a decrease in the concentration profiles.

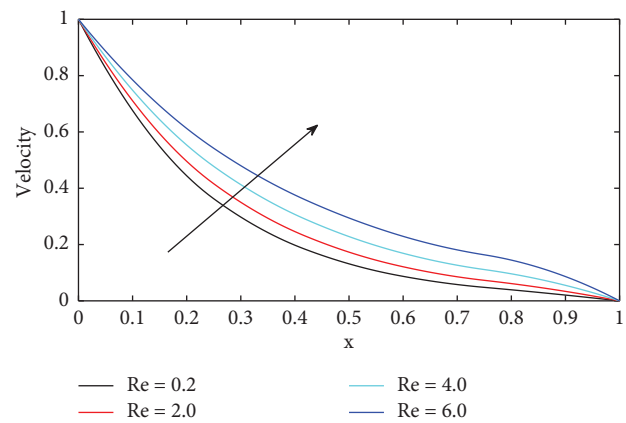

Figure 7: Velocity profiles for different values of Re.

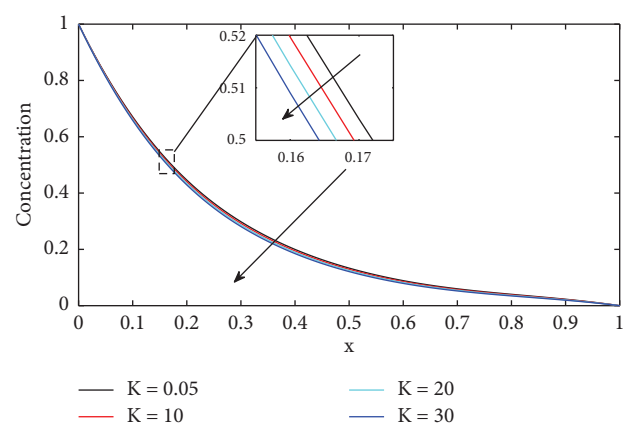

Figure 8: Concentration profiles for different values of K.

The effects of Schmidt number (Sc) on concentration Profiles are shown in Figure 10. Graphically, it is observed that the concentration profiles decrease as the Schmidt number (Sc) increases. By the definition, the Schmidt number represents the ratio of kinematic air viscosity to the mass diffusivity. Physically, increasing Schmidt number

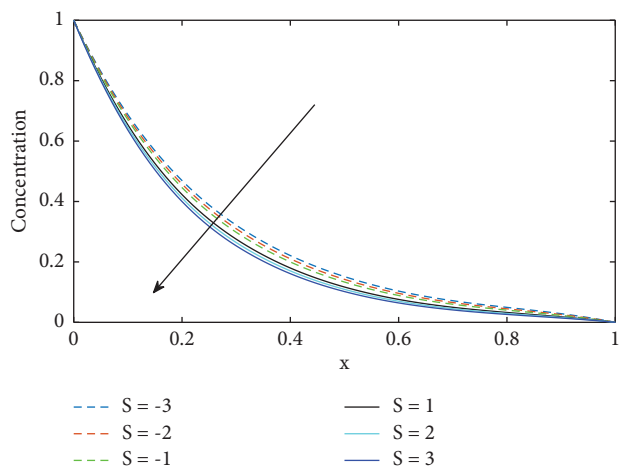

Figure 9: Concentration profiles for different values of S.

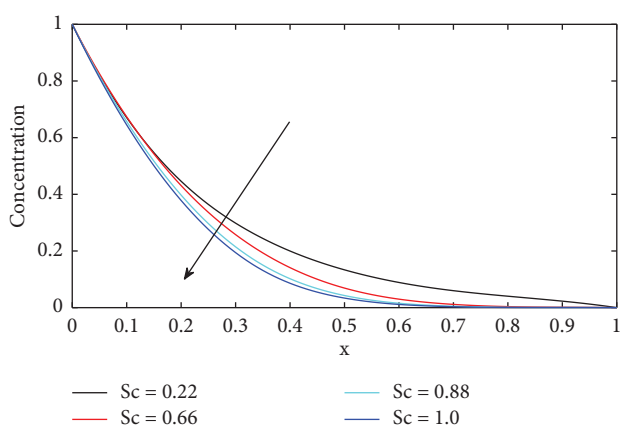

Figure 10: Concentration profiles for different values of Sc.

reduces the mass diffusivity, which results to a decrease in the concentration profiles.

The effects of magnetic Prandtl number (Prm) on induced magnetic field profiles are shown in Figures 11 and 12. Graphically, it is observed that increasing the values of the magnetic Prandtl number (Prm) leads to a decrease in the induced magnetic field profiles. Physically, increasing the magnetic Prandtl number reduces the magnetic diffusivity, which leads to a decrease in the induced magnetic field by the motion of a conducting medium and thus the induced magnetic field profiles decrease.

The effects of suction/injection parameter (S) on induced magnetic profiles are shown in Figures 13 and 14. Graphically, it is observed that increasing the values of the suction parameter (S) leads to a decrease in the induced magnetic field profiles. Increasing suction/injection parameter (S) leads to a decrease in the fluid the flow system and thus decreases the velocity of the fluid which reduces the interaction between the fluid and magnetic field and thus decreases the induced magnetic field profiles.

The effects of the Reynolds number (Re) on an induced magnetic field profiles along x–direction are shown in Figure 15. Graphically, it is observed that increasing the

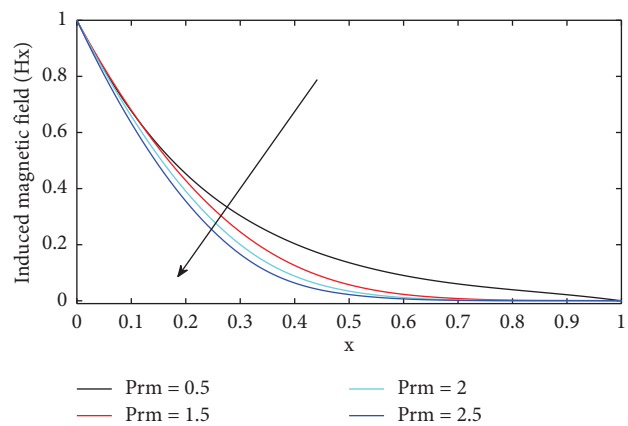

Figure 11: Induced magnetic field profiles for different values of Prm.

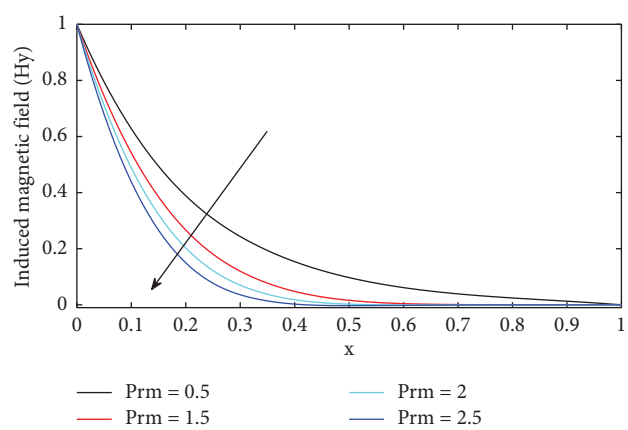

Figure 12: Induced magnetic field profiles for different values of Prm.

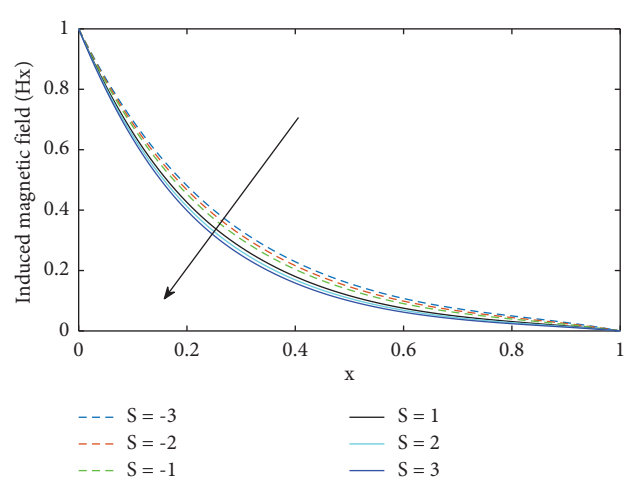

Figure 13: Induced magnetic field profiles for different values of S.

values of the Reynolds number (Re) leads to an increase in the induced magnetic field. By the definition, the Reynolds number represents the ratio of inertia force to the viscous

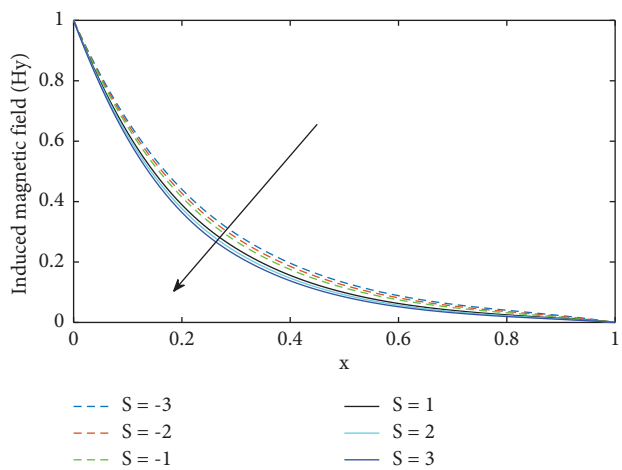

Figure 14: Induced magnetic field profiles for different values of S.

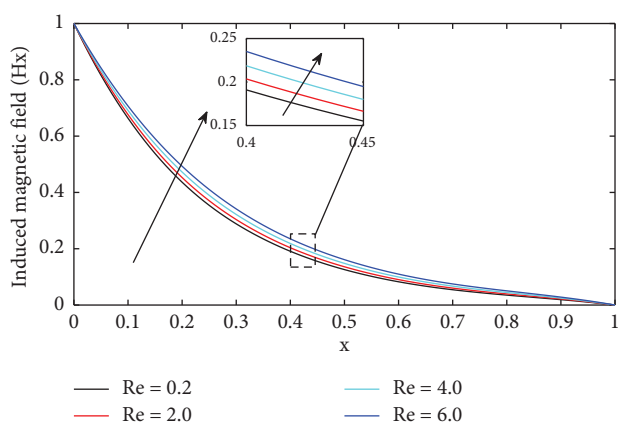

Figure 15: Induced magnetic field profiles for different values of Re
.

forces. Physically, increasing the Reynolds number reduces the viscous force which leads to an increase of interaction between the fluid and magnetic field and thus increases induced magnetic field profiles.

The effects of the Reynolds number (Re) on induced magnetic field profiles along y–direction are shown in Figure 16. Graphically, it is observed that increase in the Reynolds number (Re) leads to a decrease in the induced magnetic field. The Reynolds number represents the ratio of inertia force to the viscous forces. Physically, increasing the Reynolds number leads to a decrease of interaction between the fluid and magnetic field and thus decreases induced magnetic field profiles.

Figure 17 demonstrates the effects of suction/injection parameter (S) on temperature profiles. Graphically, it is observed that increase in the suction/injection parameter (S) leads to an decrease in the fluid temperature. Physically, increasing suction/injection parameter (S) results in the thinning of the thermal boundary layer of the fluid flow which leads to decrease the temperature profiles.

The effects of the Eckert number (Ec) on temperature profiles are shown in Figure 18. Graphically, it is observed

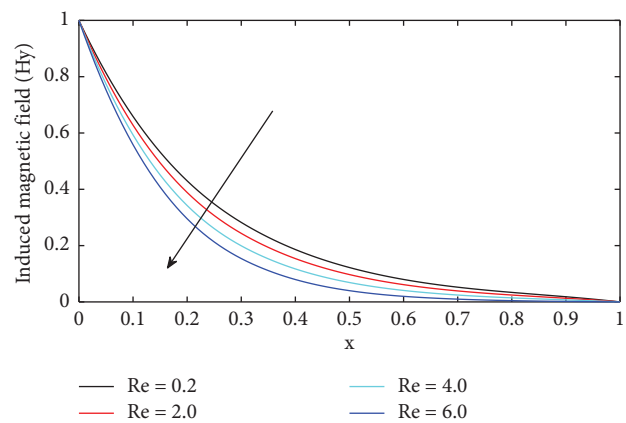

Figure 16: Induced magnetic field profiles for different values of Re
.

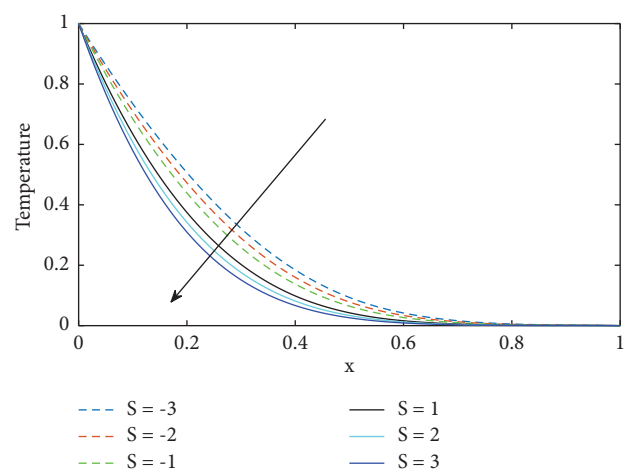

Figure 17: Temperature profiles for different values of S.

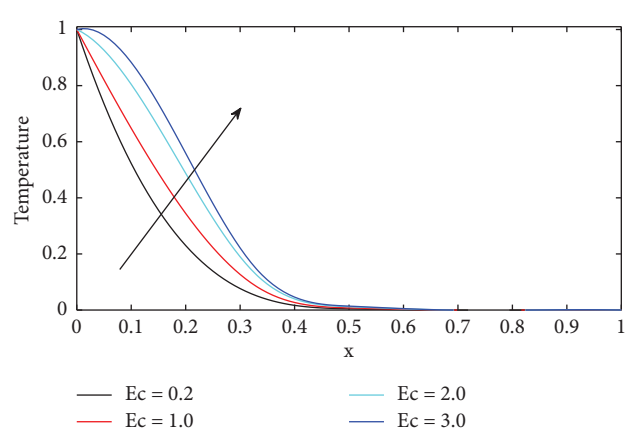

Figure 18: Temperature profiles for different values of Ec.

increasing the values of the Eckert number (Ec) leads to an increase in the temperature profile. By the definition, the Eckert number represents the ratio of the fluid flow kinetic

energy to the enthalpy of the fluid. Physically, increasing the Eckert number reduces the enthalpy of the fluid and thus increases the temperature of the fluid. The motion of the fluid increases as an increase of the Eckert number which transforms into kinetic energy which lead to an increase in the temperature profiles.

The effects of the Prandtl number (Pr) on temperature profiles are shown in Figure 19. Graphically, it is observed that the temperature of the fluid decreases as the values of the Prandtl number (Pr) increases. By the definition, the Prandtl number represents the ratio of viscous force/momentum diffusivity to the thermal diffusivity. Physically, increasing the Prandtl number reduces the thermal diffusivity and increase viscosity of the fluid which leads to an increase of temperature of the fluid.

Figure 20 illustrates the effects of varying heat generation parameter Q on temperature profiles. Graphically, it is observed that temperature profile is greatly influenced by heat generation parameter Q. Physically, increasing heat generation parameter Q leads to an increase in the temperature of the fluid. By increasing heat generation parameter Q leads to an increase in kinetic energy which leads to an increase in the thermal boundary layer and thus results to an increase in the temperature profiles.

The impacts of varying Joule heating parameter (J) on temperature profiles are shown Figure 21. Graphically, it is noticed that the temperature profiles increase with an increase in the Joule heating parameter (J). Physically, increasing the Joule heating parameter leads to an increase in the friction, and thus the mechanical energy converted into thermal energy which results to an increase in the temperature of the fluid and thus temperature profiles increase.

Table 1 shows the effects of the Prandtl number, Eckert number, heat generation parameter, and Joule heating parameter on the rate of heat transfer (Nusselt number) at the stationary and moving plates. It is observed from the table that the Nusselt number $\theta'(1)$ at the stationary plate decreases with an increase in the Prandtl number whereas increase with an increase in Joule heating parameter, heat generation parameter, and Eckert number. The Nusselt number $\theta'(0)$ at the moving plate increases with an increase in Joule heating parameter, Eckert number, and heat generation parameter whereas decrease with an increase in the Prandtl number.

Table 2 shows the effects of magnetic parameter, Prandtl number, Reynolds number, heat generation parameter, and Joule heating parameter on the wall shear stress (skin friction coefficient) at the moving and stationary plates. It is observed from the table that the wall shear stress $V^{*'}(1)$ at the stationary plate increases with an increase in the Prandtl number, magnetic parameter, and Reynolds number whereas decrease with an increase in heat generation parameter and Joule heating parameter. The skin friction coefficient $V^{*}(0)$ at the moving plate increases with an increase in the Prandtl number, magnetic parameter, and Reynolds number whereas decrease with an increase in heat generation parameter and Joule heating parameter.

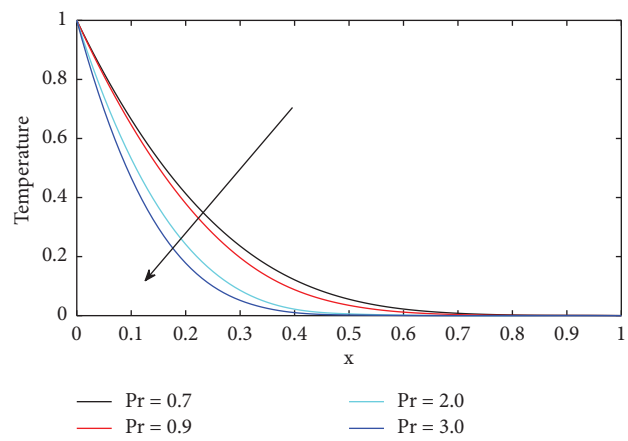

Figure 19: Temperature profiles for different values of Pr.

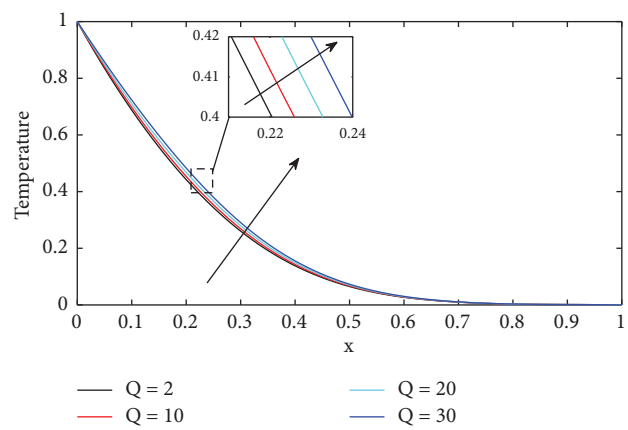

Figure 20: Temperature profiles for different values of Q.

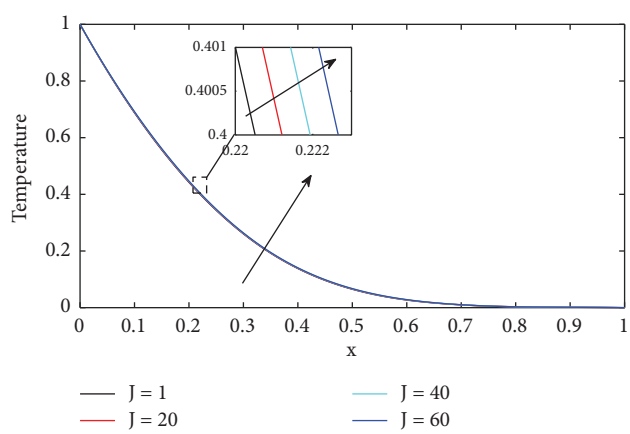

Figure 21: Temperature profiles for different values of J.

Table 3 shows the effects of Schmidt number and chemical reaction parameter on the Sherwood number at the moving and stationary plates. It is observed from the table that the rates of mass transfer (Sherwood number) at the

Table 1: Results of the Nusselt number for various values of physical parameters.

Pr	J	Ec	Q	$Nu_0 = \theta'(0)$	$Nu_1 = \theta'(1)$
0.71	1	0.2	2	0.15882500	0.10434400
0.9	1	0.2	2	0.12712400	0.07421510
2	1	0.2	2	0.02134050	0.00563502
3	1	0.2	2	0.00212662	0.00032171
	4	0.2	2	0.16084900	0.10579500
	5	0.2	2	0.16152300	0.10627800
	6	0.2	2	0.16219800	0.10676200
		0.3	2	0.16343900	0.10739100
		0.6	2	0.17728700	0.11653800
		0.9	2	0.19114500	0.12569100
			3	0.16072400	0.10622000
			4	0.16264900	0.10813600
			6	0.16658500	0.11209400

Bold values represent the variation of physical parameters.

Table 2: Results of skin-friction coefficient for various values of physical parameters.

Pr	M	Re	Q	J	$Cf_0 = V^{*'}(0)$	$Cf_1 = V^{*'}(1)$
0.71	3	2	2	1	−0.07769460	−0.03313750
0.9	3	2	2	1	−0.07739590	−0.03273990
2	3	2	2	1	−0.07613270	−0.03151520
3	3	2	2	1	−0.07559800	−0.03118010
	6	2	2	1	−0.05388150	−0.00853790
	7	2	2	1	−0.04547580	0.00026801
	8	2	2	1	−0.03682060	0.00940092
		3	2	1	−0.02733950	−0.00476105
		4	2	1	−0.00352160	0.00258175
		5	2	1	0.00346528	0.00249100
			4	1	−0.07773100	−0.03318690
			5	1	−0.07774950	−0.03321220
			6	1	−0.07776820	−0.03323800
				4	−0.07771760	−0.03316140
				5	−0.07772530	−0.03316930
				6	−0.07773290	−0.03317730

Bold values represent the variation of physical parameters.

Table 3: Results of the Sherwood number for various values of physical parameters.

K	Sc	$Sh_0 = \phi'(0)$	$Sh_1 = \phi'(1)$
0	0.22	0.25351000	0.22211800
0	0.66	0.15488300	0.10368600
0	0.88	0.11590700	0.06748990
0.05	0.22	0.25346600	0.22205700
1	0.22	0.25264000	0.22090100
2	0.22	0.25177400	0.21969100

Bold values represent the variation of physical parameters.

moving and stationary plates decrease with an increase in the chemical reaction parameter and Schmidt number.

5. Concluding Remarks

We examine the effects of chemical reaction and Joule heating on the MHD generalized Couette flow between two vertical porous plates with an induced magnetic field and Newtonian heating/cooling. The system of the governing equations of partial differential equations of the model is solved numerically using the finite difference method. The numerical results for the temperature, velocity, concentration, and induced magnetic field profiles are presented graphically for the pertinent parameters. The numerical values for skin friction coefficient, Nusselt, and Sherwood numbers are represented in the tabular form. The major findings of the present analysis can be summarized in the following points:

(i) The velocity profiles increase with rising the values of Gr, Re, and Gc while increasing M and S have an opposite effect on the velocity profiles

(ii) The temperature of the fluid increase with an increasing the values of Q, J, and Ec while increasing Pr and S leads to a decrease in the temperature fluid

(iii) The rates of heat transfer at the moving and stationary plates increases with an increase in the J, Q, and Ec while decrease with an increase in Pr

(iv) The skin friction coefficient (wall shear stress) at the stationary and moving plates increases with an increase in M, Pr, and Re while decrease with an increase in the J and Q

(v) The rate of mass transfer at the moving plate $\phi'(0)$ decreases with an increase in the K and Sc. However, at the stationary plate $\phi'(1)$ decreases with an increase in Sc and K

(vi) An increasing K, S, and Sc decrease the concentration profiles

(vii) An induced magnetic field profiles decrease with rising the values of Prm, Re, and S

Future research can be conducted on the MHD generalized Couette flow between two parallel vertical porous plates in presence of an inclined variable magnetic field.

Nomenclature

g: Acceleration due to gravity (ms^{-2})
B_0: Uniform applied magnetic field along x-axis (Wbm^{-2})
v^*: Nondimensional velocity component along y-direction
k: Coefficient of thermal conductivity $(Wm^{-1}k^{-1})$
t: Time (S)
t^*: Dimensionless time
B_y: Induced magnetic field along y-direction (T)
B_x: Induced magnetic field along x-direction (T)
$\vec{J}$: Current density (Am^{-2})
$\vec{H}$: Magnetic field strength (Am^{-1})
V: Velocity components along y axis (ms^{-1})
C_s: Concentration susceptibility (m/mole)
T_m: Mean fluid temperature (k)
T: Temperature (k)
C: Species concentration (mole/kg)
$\vec{q}$: velocity of the fluid (ms^{-1})
C_p: Specific heat at constant pressure $(JKg^{-1}k^{-1})$

T_{mp}: Temperature of the fluid in the moving plate (k)
T_{sp}: Temperature of the fluid in the stationary plate (k)
C_{mp}: Concentration of the fluid in the moving plate (mole/kg)
C_{sp}: Concentration of the fluid in the stationary plate (mole/kg)
D_m: Mass diffusivity/chemical molecular diffusivity (m^2s^{-1})
K_t: Thermal diffusion ratio (m^2s)
u_0: Injection/suction velocity (mS^{-1})
h: Distance between two parallel plates (m)
H^*: Nondimensional induced magnetic field
U: Constant velocity of the moving plate (ms^{-1})
μ: Viscosity $(Kgm^{-1}s^{-1})$
ρ: Fluid density (Kgm^{-3})
∇: Gradient operator
β_*^t: Coefficient of volume expansion for heat transfer (K^{-1})
β_*^c: Coefficient of thermal expansion for concentration gradient (m^3/mole)
σ: Electrical conductivity (Sm^{-1})
$\Delta t, \Delta x$: Time and distance intervals
θ: Nondimensional temperature
ϕ: Nondimensional concentration
ν: Kinematic viscosity (m^2s^{-1})
μ_e: Magnetic permeability (Hm^{-1})
Q: Internal heating generation parameter/Newtonian heating/cooling parameter
K: Chemical reaction parameter
k_r: Reaction coefficient
J: Joule heating parameter.

Data Availability

The data used to support the findings of this study are included within the article.

Conflicts of Interest

The author declare no conflicts of interest.

Acknowledgments

The author wish to express their very sincere thanks to anonymous reviewers for their valuable comments and suggestions.

References

[1] D. Khan, P. Kumam, A. u. Rahman et al., "The outcome of Newtonian heating on Couette flow of viscoelastic dusty fluid along with the heat transfer in a rotating frame: second law analysis," *Heliyon*, vol. 8, no. 9, Article ID e10538, 2022.

[2] J. C. Umavathi, I. C. Liu, and J. P. Kumar, "Magnetohydrodynamic Poiseuille-Couette flow and heat transfer in an inclined channel," *Journal of Mechanics*, vol. 26, no. 4, pp. 525–532, 2010.

[3] O. A. Bég, S. K. Ghosh, and M. Narahari, "Mathematical modeling of oscillatory MHD Couette flow in a rotating highly permeable medium permeated by an oblique magnetic field," *Chemical Engineering Communications*, vol. 198, no. 2, pp. 235–254, 2010.

[4] Z. Barikbin, R. Ellahi, and S. Abbasbandy, "The Ritz-Galerkin method for MHD Couette flow of non-Newtonian fluid," 2014, https://www.sid.ir/en/journal/ViewPaper.aspx?id=389767.

[5] L. Sreekala and E. K. Reddy, "Steady MHD Couette flow of an incompressible viscous fluid through a porous medium between two infinite parallel plates under effect of inclined magnetic field," *International Journal of Engineering Science*, vol. 3, pp. 18–37, 2014.

[6] K. Joseph, S. Daniel, and G. Joseph, "Unsteady MHD Couette flow between two infinite parallel porous plates in an inclined magnetic field with heat transfer," *International Journal of Mathematics and Statistics Invention*, vol. 2, pp. 103–110, 2014.

[7] S. Mosayebidorcheh, T. Mosayebidorcheh, M. Hatami, D. D. Ganji, and S. Mirmohammadsadeghi, "Investigation of transient MHD Couette flow and heat transfer of dusty fluid with temperature-dependent oroperties," *Journal of Applied Fluid Mechanics*, vol. 8, no. 4, pp. 921–929, 2015.

[8] B. K. Jha, B. Isah, and I. Uwanta, "Unsteady MHD free convective Couette flow between vertical porous plates with thermal radiation," *Journal of King Saud University Science*, vol. 27, no. 4, pp. 338–348, 2015.

[9] A. T. Ngiangia and A. Okechukwu, "Influence of variable electroconductivity and radiation on MHD Couette flow," *World Scientific News*, vol. 47, pp. 241–253, 2016.

[10] R. S. Raju, G. Jithender Reddy, J. A. Rao, and M. M. Rashidi, "Thermal diffusion and diffusion thermo effects on an unsteady heat and mass transfer magnetohydrodynamic natural convection Couette flow using FEM," *Journal of computational Design and Engineering*, vol. 3, no. 4, pp. 349–362, 2016.

[11] A. O. Ali, O. D. Makinde, and Y. Nkansah-Gyekye, "Numerical study of unsteady MHD Couette flow and heat transfer of nanofluids in a rotating system with convective cooling," *International Journal of Numerical Methods for Heat and Fluid Flow*, vol. 26, 2016.

[12] V. M. Job and S. R. Gunakala, "Unsteady MHD free convection Couette flow between two vertical permeable plates in the presence of thermal radiation using galerkin's finite element method," *International Journal of Mechanical Engineering*, vol. 2, pp. 99–110, 2016.

[13] Y. Ali, M. Rana, and M. Shoaib, ", Magnetohydrodynamic three-dimensional Couette flow of a Maxwell fluid with periodic injection/suction," *Mathematical Problems in Engineering*, vol. 2017, Article ID 1859693, 19 pages, 2017.

[14] Z. Hussain, S. Hussain, T. Kong, and Z. Liu, "Instability of MHD Couette flow of an electrically conducting fluid," *AIP Advances*, vol. 8, no. 10, Article ID 105209, 2018.

[15] E. O. Anyanwu, R. O. Olayiwola, M. D. Shehu, and A. Lawal, "Radiative effects on unsteady MHD Couette flow through a parallel plate with constant pressure gradient," *Asian Research Journal of Mathematics*, pp. 1–19, 2020.

[16] R. Kareem and J. Gbadeyan, "Entropy generation and thermal criticality of generalized Couette hydromagnetic flow of two-step exothermic chemical reaction in a channel," *International Journal of Thermofluids*, vol. 5-6, Article ID 100037, 2020.

[17] B. K. Jha and M. N. Sarki, "Chemical reaction and Dufour effects on nonlinear free convection heat and mass transfer flow near a vertical moving porous plate," *Heat Transfer*, vol. 49, no. 2, pp. 984–999, 2020.

[18] D. Soumya, B. Gireesha, and P. Venkatesh, "Planar Couette flow of power law nanofluid with chemical reaction, nanoparticle injection and variable thermal conductivity," *Proceedings of the Institution of Mechanical Engineers - Part C: Journal of Mechanical Engineering Science*, vol. 236, no. 10, pp. 5257–5268, 2022.

[19] T. S. Reddy, M. Raju, and S. Varma, "Unsteady MHD free convection oscillatory Couette flow through a porous medium with periodic wall temperature in presence of chemical reaction and thermal radiation," *Int. J. Adv. Sci. Technol*, vol. 1, pp. 51–58, 2011.

[20] A. O. Ajibade and A. M. Umar, "Effect of chemical reaction and radiation absorption on the unsteady mhd free convection Couette flow in a vertical channel filled with porous materials," *Afrika Matematika*, vol. 27, no. 1-2, pp. 201–213, 2016.

[21] A. Apelblat, "Mass transfer with a chemical reaction of the first order: analytical solutions," *The Chemical Engineering Journal*, vol. 19, no. 1, pp. 19–37, 1980.

[22] J. Prakash, K. S. Balamurugan, and S. V. Varma, "Thermodiffusion and chemical reaction effects on MHD three dimensional free convective Couette flow," *Walailak Journal of Science and Technology*, vol. 12, pp. 805–830, 2015.

[23] M. Abbaszadeh, M. Bayat, M. Dehghan, and M. I. Azis, "Investigation of generalized Couette hydromagnetic flow of two-step exothermic chemical reaction in a channel via the direct meshless local petrov–galerkin method," *Engineering Analysis with Boundary Elements*, vol. 125, pp. 178–189, 2021.

[24] Z. Chen and P. Arce, "An integral-spectral approach for convective-diffusive mass transfer with chemical reaction in Couette flow mathematical formulation and numerical illustrations," *Chemical Engineering Journal*, vol. 68, no. 1, pp. 11–27, 1997.

[25] B. C. Sarkar, "Laminar forced convection mhd Couette-Poiseuille flow with viscous and joule dissipations," *Journal of Scientific Research (Indonesia)*, vol. 14, no. 3, pp. 877–889, 2022.

[26] J. Zueco, O. A. Bég, and L. L. Ochoa, "Non-linear transient hydromagnetic partially ionised dissipative Couette flow in a non-darcian porous medium channel with hall, ionslip and joule heating effects," *Progress in Computational Fluid Dynamics, an International Journal*, vol. 11, no. 2, pp. 116–129, 2011.

[27] K. Ramesh, "Effects of viscous dissipation and joule heating on the Couette and Poiseuille flows of a jeffrey fluid with slip boundary conditions," *Propulsion and Power Research*, vol. 7, no. 4, pp. 329–341, 2018.

[28] O. A. Bég, J. Zueco, and H. S. Takhar, "Unsteady magnetohydrodynamic hartmann–Couette flow and heat transfer in a darcian channel with hall current, ionslip, viscous and joule heating effects: network numerical solutions," *Communications in Nonlinear Science and Numerical Simulation*, vol. 14, no. 4, pp. 1082–1097, 2009.

[29] C. A. Saleel, S. A. Alshahrani, A. Afzal, M. A. A. Baig, S. Kamangar, and T. Y. Khan, "Flow control in microfluidics devices: electro-osmotic Couette flow with joule heating effect," *Frontiers in Engineering and Built Environment*, vol. 1, 2021.

[30] M. Shamshuddin, S. R. Mishra, O. A. Bég, and A. Kadir, "Viscous dissipation and joule heating effects in non-fourier mhd squeezing flow, heat and mass transfer between riga plates with thermal radiation: variational parameter method solutions," *Arabian Journal for Science and Engineering*, vol. 44, no. 9, pp. 8053–8066, 2019.

[31] M. D. Shamshuddin and P. V. Satya Narayana, "Combined effect of viscous dissipation and joule heating on mhd flow past a riga plate with cattaneo–christov heat flux," *Indian Journal of Physics*, vol. 94, no. 9, pp. 1385–1394, 2020.

[32] Sarveshanand and A. Singh, "Magnetohydrodynamic free convection between vertical parallel porous plates in the presence of induced magnetic field," *SpringerPlus*, vol. 4, pp. 1–13, 2015.

[33] J. Mng'ang'a, M. Kinyanjui, and E. R. Onyango, "Hydromagnetic surface driven flow between two parallel vertical plates in the presence of chemical reaction and induced magnetic field," *Global Journal of Pure and Applied Mathematics*, vol. 18, pp. 583–612, 2022.

[34] J. K. Kwanza and J. A. Balakiyema, "Magnetohydrodynamic free convective flow past an infinite vertical porous plate with magnetic induction," *Journal of Fusion Energy*, vol. 31, no. 4, pp. 352–356, 2012.

[35] R. K. Singh, A. K. Singh, N. C. Sacheti, and P. Chandran, "On hydromagnetic free convection in the presence of induced magnetic field," *Heat and Mass Transfer*, vol. 46, no. 5, pp. 523–529, 2010.

[36] N. S. Akbar, M. Raza, and R. Ellahi, "Interaction of nanoparticles for the peristaltic flow in an asymmetric channel with the induced magnetic field," *The European Physical Journal Plus*, vol. 129, no. 7, pp. 155–212, 2014.

[37] N. Sher Akbar, M. Raza, and R. Ellahi, "Influence of induced magnetic field and heat flux with the suspension of carbon nanotubes for the peristaltic flow in a permeable channel," *Journal of Magnetism and Magnetic Materials*, vol. 381, pp. 405–415, 2015.